Haptic Perception of Virtual Bumps Displayed Through a Piezo-Actuated Touch Screen

by

Buket Baylan

A Thesis Submitted to the

Graduate School of Sciences and Engineering

in Partial Fulfillment of the Requirements for

the Degree of

Master of Science

in

Mechanical Engineering

Koc University

October, 2014

Koc University

Graduate School of Sciences and Engineering

This is to certify that I have examined this copy of a master's thesis by

Buket Baylan

and have found that it is complete and satisfactory in all respects,
and that any and all revisions required by the final
examining committee have been made.

Committee Members:

_____

Prof. Çağatay Başdoğan

_____

Assoc. Prof. İpek Başdoğan

_____

Assoc. Prof. Özgür Birer

Date: _____

Anneme, Babama ve Kardeşime
Mine Baylan, Yalçın Baylan, Demet Baylan

ABSTRACT

This thesis aims to design a piezo-actuated touch screen for displaying vibrotactile haptic feedback. We have designed a touch screen to display haptic bumps to a user via four rectangular piezo patches attached to its surface. Using a finite element (FE) model, the dimensions of the screen and the appropriate boundary conditions are determined carefully based on the range of vibration frequencies detectable by a human finger. Then, the optimum configuration (location and orientation) for the piezo patches is determined such that the vibration amplitude of the screen is maximized for a unit voltage applied to each piezo patch. Our FE analysis shows that the best output is obtained when the piezo actuators are placed close to the boundaries and not the free edges. In order to validate the results obtained through the FE model, an experimental modal analysis of the glass plate is also performed using a laser Doppler vibrometer (LDV). Following the design and characterization of the plate, we have investigated the effect of displaying haptic bumps through the plate on human perception of roughness by conducting psychophysical experiments with 10 subjects. To generate the desired haptic bumps displayed to the subjects, the high frequency vibrations of the plate at its first resonance frequency is modulated with desired low frequency unipolar pulse waves in different shape (sinusoidal, square, sawtooth), peak amplitude, duty cycle, and spatial frequency. The subjects are asked to rate their tactile perception of 81 different haptic bumps on a Likert scale of 1-7 using the adjectives of smooth-rough and flat-bumpy. The results of the user study show that the perceived roughness increases with increasing peak amplitude, duty cycle, and spatial frequency. The subjects perceived the square wave as the roughest while the sawtooth was perceived as the smoothest among 3 waveforms. It is also observed that there is a close relation between the root mean square (RMS) values of the signals and roughness perception. Perception of roughness increases as the RMS values of the signals increases.

ÖZETÇE

Bu tezin amacı, titreşim bazlı dokunsal geribildirim sağlamak için piezoelektrik eyleyiciler aracılığıyla uyarılan dokunmatik bir ekran tasarlamak ve bu düzenek aracılığıyla insanların pürüzlülük algısını ölçmektir. Cam ekran yüzeyine yapıştırılan dört piezoelektrik eyleyici aracılığıyla, kullanıcıya dokunsal tümsekler görüntüleyecek bir dokunmatik ekran tasarlanmıştır. Sonlu elemanlar modeli kullanılarak sistem için uygun ekran boyutları, sınır koşulları ve piezoelektrik eyleyiciler için ideal konfigürasyon belirlenmiştir. Sınır koşullarının belirlenmesinde insan parmağı tarafından algılanabilen titreşim frekans aralığı dikkate alınmıştır. İdeal konfigürasyon seçiminde ise piezoelektrik eyleyicilere uygulanan birim voltaj karşılığı ekranda elde edilen maksimum titreşim genliği esas alınmıştır. Analiz sonuçları en iyi verilerin piezo eyleyiciler sınırlara yakın yerleştirildiği zaman elde edildiğini göstermiştir. Cam levhanın lazer-Doppler titreşim-ölçer aracılığıyla deneysel modal analizi gerçekleştirilmiş ve bu sonuçlar sonlu eleman modeli aracılığıyla elde edilen sonuçlarla karşılaştırılıp doğrulanmıştır. Cam levhanın tasarımı ve karakterizasyonunun ardından 10 kişi ile psikofiziksel deneyler yapılmıştır. Bu deneylerde cam levha üzerinde oluşturulan dokunsal tümsekler aracılığıyla insanların pürüzlü yüzey algısı araştırılmıştır. Levhanın ilk rezonansına karşılık gelen yüksek frekanslı titreşimler ile farklı şekil (sinüs, kare, testere dişi dalga), genlik, görev döngüsü ve uzay frekansına sahip, düşük frekanslı, tek kutuplu nabız dalgaları modüle edilerek, deneklere iletilecek olan dokunsal tümsekler yaratılmıştır. Deneklerden dokunsal algılarını pürüzsüz-pürüzlü ve düz-inişli çıkışlı sıfatlarını kullanarak Likert ölçeğinde 1-7 arasında derecelendirmeleri istenmiştir. Deneklerle gerçekleştirilen deneylerin sonuçları pürüzlülük algısının genlik, görev döngüsü ve uzaysal frekansındaki artışla doğru orantılı olduğunu göstermiştir. Denekler üç dalga çeşidi arasından kare dalgayı en pürüzlü, testere dişi dalgayı ise en pürüzsüz olarak algılamışlardır. Bunların yanında sinyallerin karekök ortalama değerleri (rms) ile pürüzlülük algısının doğru orantılı olduğu da gözlenmiştir.

I am deeply grateful to Ömer Şirin for his everlasting support and encourage. He was a great source of motivation and I will always be grateful to him for all the things he had done for me.

I am indepted to Mehmet Ayyıldız, Soner Cinoğlu, Ozan Çaldıran, Utku Boz, Ümmü Koç, Murat Gözüm and Mahmut Biçer for their friendship. I will be missing our coffee hours and all the conversations and fun we had together. I am so lucky to have friends like them.

I also want to thank my lab colleagues Ayşe Küçükyılmaz, Ezgi Emgin, Yusuf Aydın, Berkay Yarpuzlu, Enes Salman, Ehsan Sadraei, Mohammad Ansarin, Nasser Arghavani and Khurram Saleem for their friendship and collaboration.

I thank my other friends from Koç University, Çağla Çığ, Banuçiçek Gürcüoğlu, Atakan Arasan, Aysu Altun and Güneş Yılmaz for their friendship and İpek Mumcu for being an enjoyable homemate to me.

I must also express my deepest gratitude to my cousin Arzu Demirbağ and beloved friends Merve Gizem Bozkurt, Yağmur Hazal Şadırvan, Gizem Tokatlı, Duygu İşibol, Merve Özdemir and Murat Menevşe. I am deeply thankful to them for their priceless friendship and invaluable support in any area of my life.

I cannot thank to my parents Mine Baylan and Yalçın Baylan enough for their unconditional support throughout this period. It would be impossible to continue without their love, patience, guidance and respect to my decisions. I love you so much and feel so lucky to have such a family.

Finally, I would like to thank to my sister Demet Baylan for being the coolest and funniest sister ever. Her presence has always been the biggest source of happiness for me and her support and trust has been one of my biggest motivations.

TABLE OF CONTENTS

LIST OF TABLES

NOMENCLATURE

ANOVA	analysis of variance
DAQ	data acquisition
FE	finite element
FRF	frequency response function
GW	groove width
LDV	laser Doppler vibrometer
RMS	root mean square
RW	ridge width
A	peak amplitude
c	elasticity matrix
D	electrical displacement vector
DC	duty cycle
e	piezoelectric constants matrix
E	electric field vector
F	externally applied force
f_1, f_2, f_3	first three resonance frequencies
f_c	frequency of the carrier signal
f_d	frequency of the desired signal
K_{uu}	stiffness matrix
$K_{u\phi}, K_{\phi u}$	piezoelectric coupling matrices
$K_{\phi\phi}$	capacitance matrix
M	mass matrix

n	wave form
NB	number of bumps
S	strain vector
T	stress vector
U	displacement
V	applied voltage
ω	angular frequency
ε	matrix of dielectric constants
φ	electrical potential
λ	wave length

Chapter 1

INTRODUCTION

Touch screens have been used over a wide range of portable devices nowadays, but our interactions with these devices mainly involve visual and auditory sensory channels, which are already overloaded. While a commercial touch screen can detect finger position, it does not provide the user with haptic feedback. However, it is known that our fingers are sensitive to electrotactile or vibrotactile stimulus in varying peak amplitude, duration and frequency. Hence, haptic feedback can be used in touch screens as an additional sensory channel to convey information and also lighten the perceptual and cognitive load of the user.

The research groups working in this area have proposed and designed haptic feedback systems based on either electrostatic or electromechanical actuation. Kaczmarek et al. [1] developed an electrode based system to produce electrostatic actuation. The electrodes were coated to prevent direct contact of the finger with them and they were arranged as a 7×7 matrix forming a square pattern. The aim was to investigate the effect of polarity of the pulses on the perceptual sensitivity. The results of the study showed that the sensitivity of the subjects to the positive pulses was less than that of the negative or biphasic pulses. Yamamato et al. [2] developed a telepresentation system for tactile exploration of remote surface textures. This system was made of two parts: a tactile sensor on the slave site and a tactile display utilizing an electrostatic actuator on the master site. As the user moves her/his finger on the display, the tactile sensor simultaneously scans the texture surface and the surface roughness recorded by the sensor is displayed to the user through the tactile display by applying two-phase cyclic voltage patterns to the electrodes. They conducted a

user study and reported that the subjects correctly matched the textures at the remote site to the local ones with a success rate of 79%. Bau et al. [3] from Disney Research developed TeslaTouch working with the electrostatic actuation principle. They controlled the frictional force between the user finger and the touch screen by modulating the frequency and the amplitude of the electrostatic force. The disadvantage of the electrostatic actuation method is that haptic feedback can be displayed to user only when her/his finger is moving on the touch screen. To provide haptic feedback to a stationary finger, electromechanical actuation (electric motors or piezo actuators) have been utilized. Fukimoto and Sugimura [4] presented the concept of "active click" on touch panels, which utilizes electric motors, integrated into a PDA, to display button click effect. They suggested that active click can improve the usability of touch panels, especially in noisy environments. Kim and Kim [5] developed a haptic processor that can control multiple electric motors to create a vibrotactile wave, traveling on a touch screen. While an electric motor is compact, cost effective, and easy to integrate into a touch screen, it operates in a narrow frequency range, limiting its bandwidth. To be able to use a wide range of actuation frequencies and hence to create richer haptic effects, piezo actuators are preferred over electric motors. The piezo actuators are also compact and can be easily mounted on a touch screen, but typically require higher voltage input. Biet et al. [6] used piezo actuators to create squeeze film effect between the user's finger and the surface of a touch screen by actuating the piezos at ultrasonic frequencies. By controlling the thickness of the squeeze film, square gratings were simulated. Giraud et al. [7] designed a haptic knob using a similar principle. Winfield et al. [8] developed TPaD by attaching a piezo disk to a glass plate. Again, ultrasonic frequencies are used to modulate the friction coefficient between the user's finger and the plate surface. Chubb et al. [9] further extended this idea in ShiverPaD by oscillating the plate in-plane via a voice coil. Hence, the ShiverPaD is capable of applying and controlling shear force on a finger regardless of its direction of motion. Dai et al. [10] designed

LateralPaD that can generate active lateral forces on a bare finger by creating simultaneous out-of-plane and in-plane vibrations on the plate surface.

Our work focuses on displaying vibrotactile haptic effects to a user through a touch screen via electromechanical actuation principle. We believe that the haptic effects that can be displayed through the touch screens will be richer and more engaging as the number and the quality of the vibration actuators attached to them increase. On the other hand, the engineering design of such systems will be highly challenging due to technological constraints (such as high power consumption) and the constraints associated with the human tactile perception. In this paper, we present a methodology based on finite element modeling (FEM) and experimental modal analysis for end-to-end design of touch screens for displaying vibrotactile haptic feedback via multiple piezo patches attached to the screen. To our knowledge, such a systematic analysis based on FEM approach has not been performed to date. The FEM approach is used to select screen dimensions, appropriate boundary conditions, and the piezo configurations (location and orientation) on the screen for achieving optimum performance within the limits of human haptic perception.

The proposed design approach enables us to generate programmable out-of-plane vibrations on the touch screen to display a rich set of haptic effects to a user. To generate various haptic effects displayed through the screen, we modulate the high frequency out-of-plane vibrations of the plate at first resonance frequency (carrier signal) with low frequency waves in different shape (sinusoidal, square, and sawtooth), peak amplitude, and duty cycle. The concept of amplitude modulation for generating vibrotactile effects is not new (Maeno et al. [11], Brown et al. [12], Ahmaniemi et al. [13], Park and Choi [14]). In these studies, the vibrations are displayed by a vibrotactile actuator held by a user. Hence, either the signal has no spatial component or the haptic feedback is passive. On the other hand, in our approach, the vibrotactile haptic effects are displayed to the finger of a user moving on the glass plate. Hence, our haptic feedback is active. Also, our vibrotactile

stimuli have components in both time and spatial domains since we alter the number of bumps displayed to the user according to the finger velocity. As a result, haptic patterns (in the form of out-of-plane vibrations) that are different along the long and short edges of the touch screen can be generated by altering the parameters used to create the vibrotactile stimuli.

Such a rich set of haptic effects can be used for various applications including, communication, games and entertainment, education, data visualization, and interface development for blinds. We imagine that haptic effects can be used to send a personal message to loved ones in the form of a beating heart, to select the fabric of a cloth by touching and feeling its textures during online shopping, to teach mathematics to primary school students (e.g. dragging one number to the other to obtain the desired sum while feeling haptic resistance for incorrect matching), to differentiate the feel of riding a bicycle on smooth, bumpy, and sandy roads during game playing, to design a haptic user interface (e.g. dragging folders and differentiate the amount of data in them based on the haptic resistance).

This thesis is organized as follows: We introduce our piezo-actuated touch screen and discuss its design details in Section 2. In Section 3, the methods for displaying haptic effects through the touch screen are explained. In Section 4, the stimuli and the experimental design are presented. In section 5, results of the experiments are given. Finally, the discussion of the results and the conclusions are given in section 6 and 7 respectively.

<div align="center">

Chapter 2

METHODS AND MATERIALS

</div>

2.1 Design of our Touch Screen

In order to construct the system shown in Figure 2.1, we first decided on the type of thin-film piezo actuators and then purchased them from the manufacturer (PI DuraAct P-876.SP1). In addition to being compact, this type of piezo-electric patches are lightweight, hence the additional weight due to coupling with the glass plate shown in Figure 2.1 is negligible compared to the own weight of the plate. Besides these advantages, the insulation layer enables it to be attached to the glass plate easily.
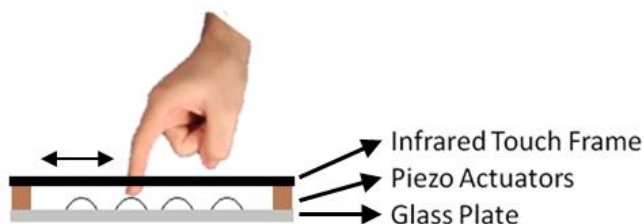
Figure 2.1: Our vibrotactile touch screen: The user feels the vibrotactile effects in the form of bumps generated by piezo actuators glued on a glass screen as she/he actively moves her/his finger on the screen. The magnitude, spatial frequency, duty cycle, and the shape of the bumps can be altered to induce application-specific tactile sensations on the user.

We glued one of the piezo patches on a glass plate and conducted some initial experiments by applying alternating voltage to the piezo patch through a signal generator and an amplifier to vibrate the glass plate. We observed that the vibrations are localized

around the attached piezo patch and a single patch is not sufficient to vibrate the whole plate. Hence, we decided to investigate the optimum number and placement of piezo patches on the glass plate. Currently, there are no established methods on a) how many piezo patches must be used and b) how they must be attached to a touch screen to generate the desired haptic effects. Since the piezo patches cannot be easily detached from the glass plate once they are glued to its surface, it is more convenient to make this analysis in a simulation environment using a finite element package. For this purpose, we developed the models of the glass plate, the piezo patch actuators attached to it, and the interactions between them in ABAQUS and then investigated the design trade-offs based on the amplitude and frequency of the vibrations of the glass plate for 8 different configurations of the piezo actuators [15]. By running simulations in ABAQUS, we first investigated the effect of 3 different boundary conditions on the resonance frequency of the plate and then the effect of piezo locations and orientations on the amplitude of the vibrations of the plate per unit voltage applied to the piezo patches. For the glass plate and the piezoelectric actuators, element types C3D20 and C3D20E are used respectively. The material properties of the glass plate are taken from the literature and given in Table 2.1 and the properties of the piezoelectric actuator patch can be found from the manufacturer's website.

First step of the design process was to perform modal analysis using ABAQUS to obtain the appropriate boundary condition that provides the smallest resonance frequencies so that the vibrations created at these frequencies can be detected by human finger. The results of the modal analysis for 3 different boundary conditions, which are a) the glass plate fully clamped, b) the long edges of the glass plate are clamped while the short edges are free, and c) the short edges of the glass plate are clamped while the long edges are free, are shown in Table 2.2. Since it is desired to vibrate the glass plate within the human perception limits (0.1-500 Hz) [16] and it would be preferable to include more resonance

frequencies within this limit to obtain richer effects, third boundary condition is chosen and a frame which fixes the short edges of the glass plate is designed for the experimental setup.

Table 2.1: Material properties of the glass plate used in the FE simulations

Density (kg/m3)	2500
Young's modulus (GPa)	70
Poisson's ratio	0.24
Structural damping (%)	0.01
Dimensions (mm)	$206 \times 147 \times 1.4$

Table 2.2: The first three resonance frequencies of the glass plate for the 3 different boundary conditions

Boundary Conditions	First Resonance (Hz)	Second Resonance (Hz)	Third Resonance (Hz)
a)	378	776	1171
b)	307	410	651
c)	158	244	541

After selecting the appropriate boundary condition, we focused on selection of the piezoelectric actuator configurations. Our design consists of four piezoelectric actuator patches attached to the glass plate in 8 different configurations (C1-C8 in Figure 2.2). To investigate the effect of piezo configurations (location and orientation) on the displacement output of the glass plate, out of plane displacements were calculated at 25 grid points (5 × 5) on its surface using the FE model and then the FRF (frequency response function) of each point was calculated for the 8 different piezo configurations.

Since mechanical and electrical energy are coupled for piezoelectric materials, constitutive equations are used to represent their behaviors. These equations are derived using conservation of energy principle and given as [17]:

$$T = c \times S - e \times E \tag{1}$$

$$D = e^T \times S + \varepsilon \times E \tag{2}$$

where T is the stress vector, c is the elasticity matrix, S is the strain vector, e is the piezoelectric constants matrix, E is the electric field vector, D is the electrical displacement vector, and ε is the matrix of dielectric constants. These matrices are entered to the ABAQUS to model the piezoelectric patches [18] (see Appendix A).

The ABAQUS model utilizes the well-known Hooke's law between stress and strain extended by piezoelectric coupling. The electro-elastic response of the glass plate to the applied voltage is governed by the following finite element equations [19]:

$$M\ddot{U} + K_{uu}U + K_{u\Phi}\Phi = F \tag{3}$$

$$K_{\Phi u}U + K_{\Phi\Phi}\Phi = V \tag{4}$$

where, M is the mass matrix, K_{uu} is the stiffness matrix, $K_{u\Phi}$ and $K_{\Phi u}$ are the piezoelectric coupling matrices, $K_{\Phi\Phi}$ is the capacitance matrix, U is the displacement, Φ is the electrical potential, F is the externally applied force and V is the applied voltage. In our case only voltage is applied and the externally applied force is zero. Substituting zero for F into (3),

$$M\ddot{U} + K_{uu}U + K_{u\Phi}\Phi = 0 \tag{5}$$

$$M\ddot{U} + K_{uu}U = -K_{u\Phi}\Phi \tag{6}$$

and solving for Φ using (4), we obtain

$$\Phi = K_{\Phi\Phi}^{-1}[V - K_{u\Phi}{}^{T}U] \tag{7}$$

Then, substituting (7) into (6), the following relation is obtained,

$$M\ddot{U} + K_{uu}U = -K_{u\Phi}K_{\Phi\Phi}^{-1}V + K_{u\Phi}K_{\Phi\Phi}^{-1}K_{u\Phi}{}^{T}U \tag{8}$$

$$M\ddot{U} + \left[K_{uu} - K_{u\Phi}K_{\Phi\Phi}^{-1}K_{u\Phi}{}^{T}\right]U = -K_{u\Phi}K_{\Phi\Phi}^{-1}V \tag{9}$$

which can be written as

$$M\ddot{U} + KU = T_{V\Phi}V \tag{10}$$

where,

$$K = K_{uu} - K_{u\Phi}K_{\Phi\Phi}^{-1}K_{u\Phi}{}^{T} \tag{11}$$

$$T_{V\Phi} = -K_{u\Phi}K_{\Phi\Phi}^{-1} \tag{12}$$

Equation (8) defines the relation between the applied voltage (V) to the piezo actuators and the resulting displacement (U) in the glass plate. Applied voltage creates a potential difference in the piezo actuators, which causes the actuator to bend and the host structure (the glass plate) to deform. Hence, if the voltage is applied to the piezo patches in the form of a sinusoidal signal

$$V = |V|e^{j\omega t} \tag{13}$$

the resulting displacements in the glass plate will be also sinusoidal

$$U = |U|e^{j\omega t + \Psi} \tag{14}$$

Then, we can obtain the frequency response function (FRF) as

$$H(\omega) = U(\omega)/V(\omega) \qquad\qquad (15)$$

FRF represents the output spectrum of a system in response to an input in ranging frequencies, and is used to characterize the dynamical response of the system.

A sinusoidal signal corresponding to amplitude of 50 Vpp is applied to the patches and the displacements are measured in microns. The vibration amplitudes for the center point of the plate are given in Figure 2.3. If the vibration amplitudes for the first 3 vibration modes are considered, third, fourth, and fifth piezo configurations are more favorable. This result suggests that the patches must be placed close to the fixed edges of the touch screen and not close to its free edges to maximize the displacement output. More details on this analysis can be found in our earlier publication [15].
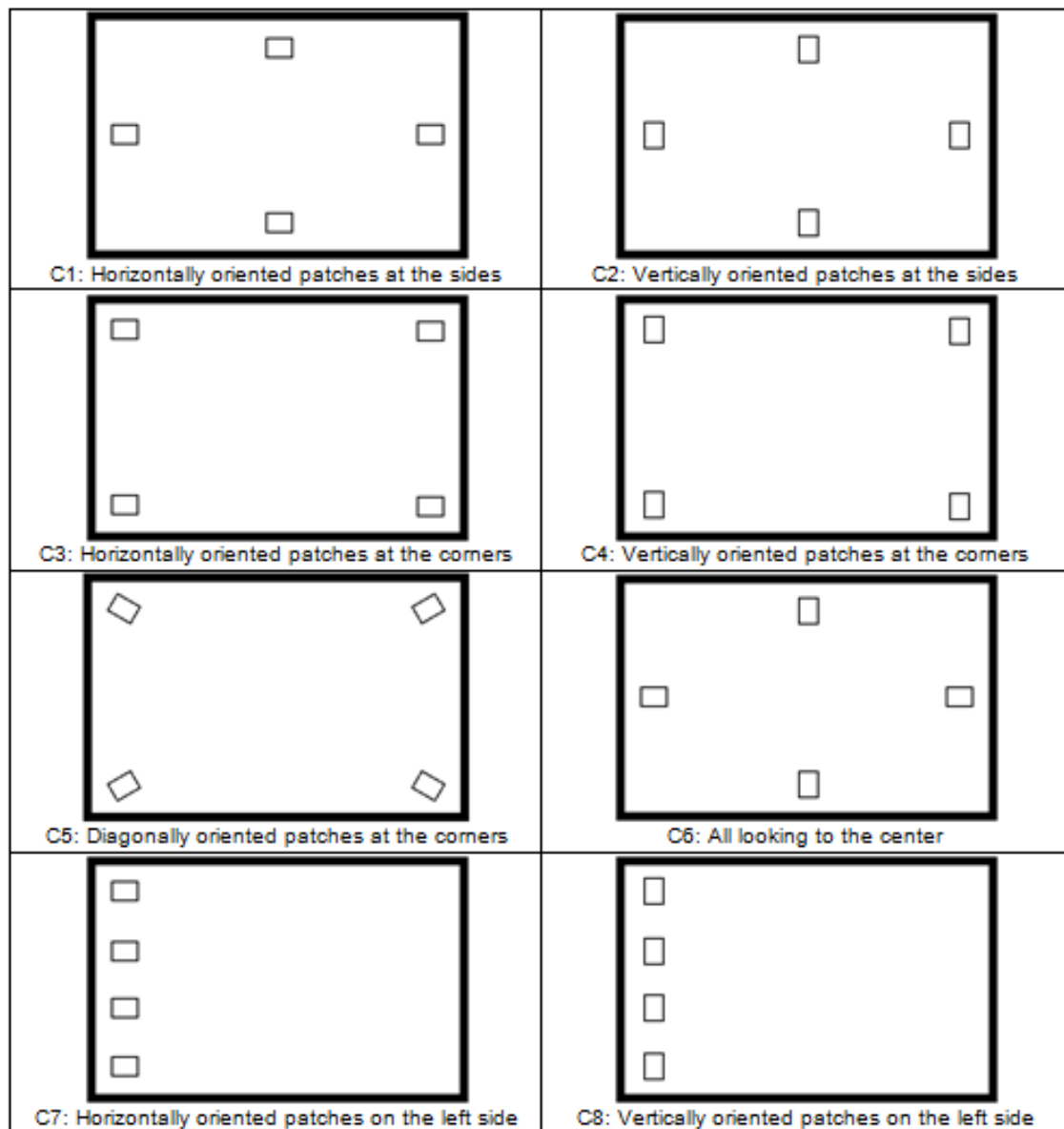
Figure 2.2: The configurations tested for the piezoelectric patches in the FE model.
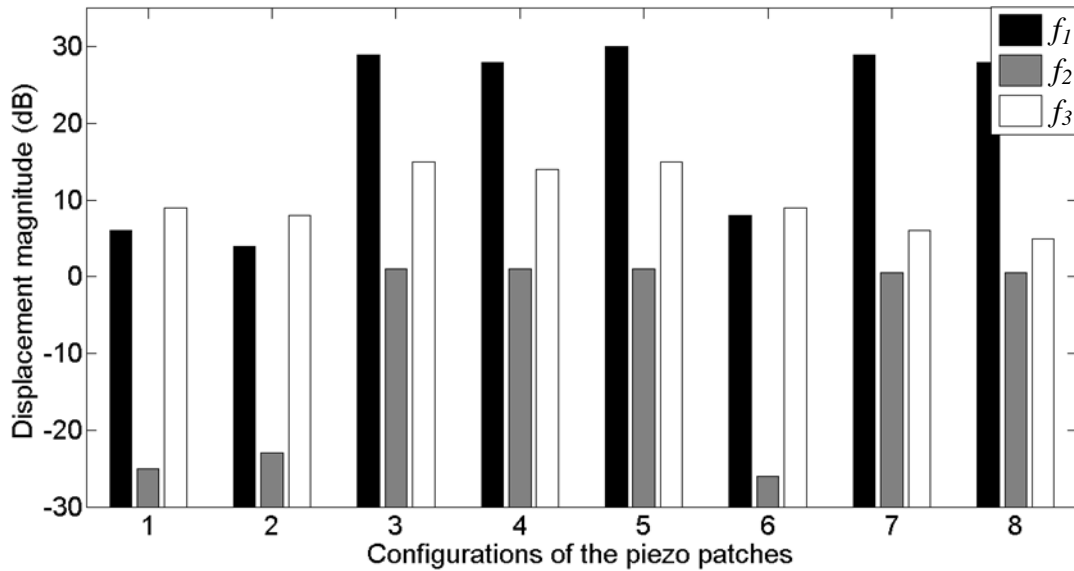
Figure 2.3: The displacement magnitudes of the first three resonances of the glass plate for 8 different configurations.

2.2 Experimental Validation

To validate the results obtained through the FE model, experimental modal analysis of the glass plate is performed (Figure 2.4). To obtain the FRFs experimentally at the grid points of the glass plate, we used the frequency sweep approach. The glass plate is actuated by applying a sinusoidal voltage (input) with an amplitude of 50Vpp to the patches via a high voltage amplifier (Model: E-413 DuraAct Piezo Driver, PI systems) in the frequency range of 1-625 Hz and the vibrational velocity (output) is measured by a LDV at the same 25 grid points on the glass plate used for the FE analysis. The collected data is processed through NetDB signal analysis software to obtain the FRFs at the grid points. Using the

experimental FRFs, the resonance frequencies of the plate and its mode shapes (i.e. deflection profiles) at those resonance frequencies are determined. The FRF data collected through NetDB software at the grid points is interpolated using a MATLAB script to display the first three mode shapes of the glass plate as shown in Figure 2.5 (bottom row). When they are compared with the ones obtained from the FE model, a close match is observed. The FRFs of the grid points A and B (see Figure 2.4(b)), where point A is at the center, are shown in Figure 2.6 for the first three resonance frequencies. Since the center point A lies along the nodal line in the second resonance mode (see Figure 2.5), the second resonance is observed at point B only.
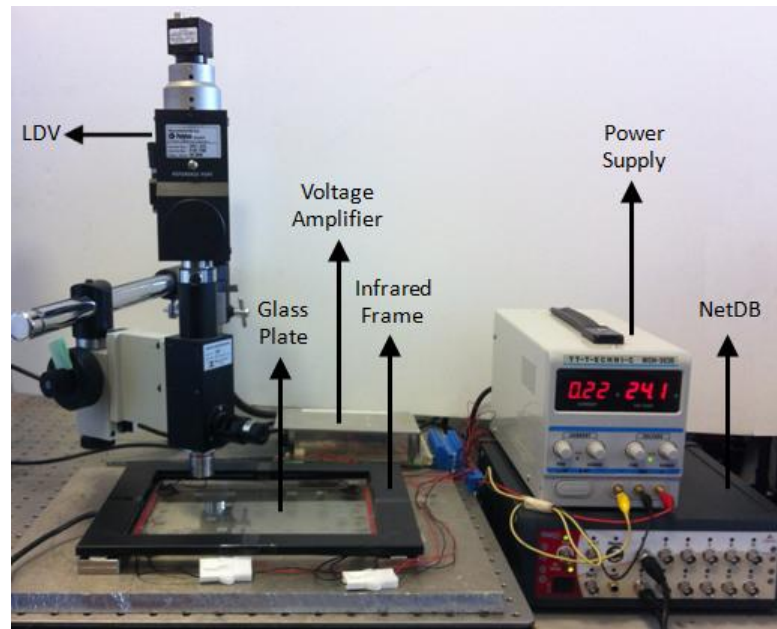
(a)
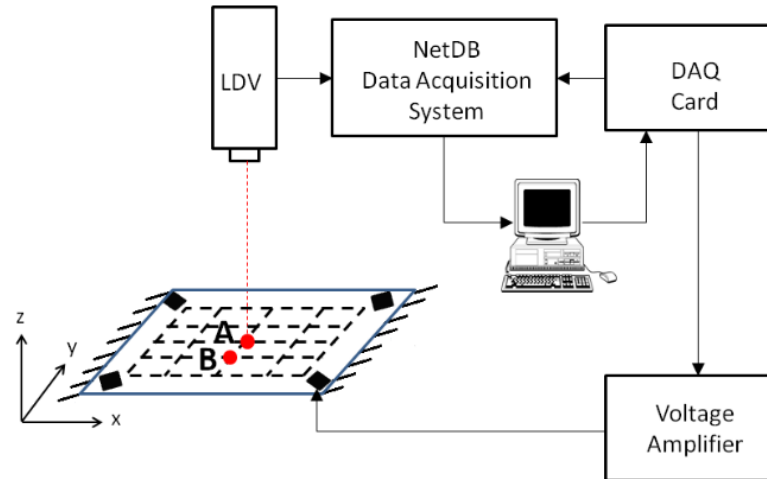
(b)

Figure 2.4: (a) The experimental set-up used for experimental modal analysis. (b) The data flow in our measurements.
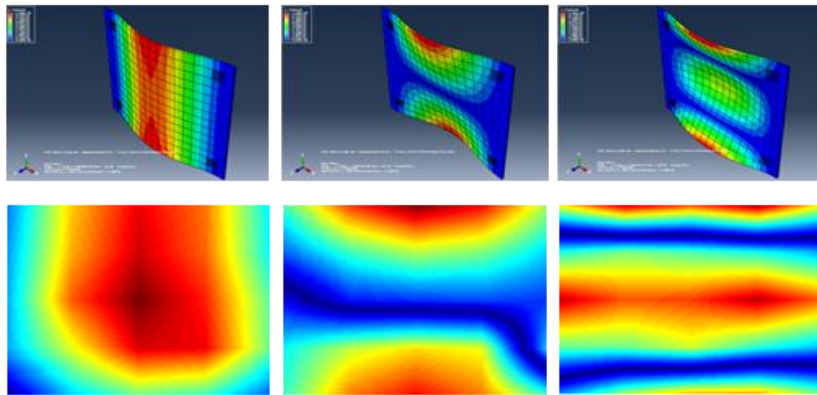
Figure 2.5: Comparison of the first three mode shapes obtained by FEM (upper row) with the experimental ones (bottom row).
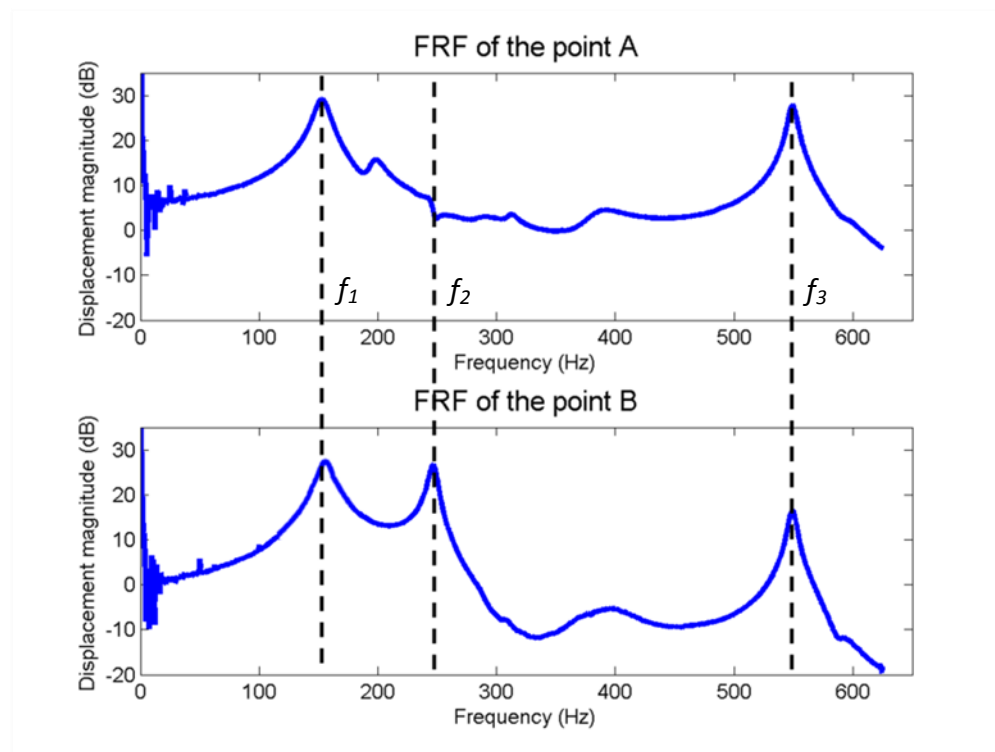
Figure 2.6: The frequency response functions of the grid points A and B. The first three resonance frequencies of the plate are $f_1 = 158$ Hz, $f_2 = 246$ Hz, and $f_3 = 548$ Hz.

Chapter 3

HAPTIC EFFECTS

Following the design and characterization of our touch screen, our work is focused on displaying haptic bumps to a user through the glass plate. At first, we realize that it is important to make the user feel the same haptic effects on the glass surface independent of her/his finger velocity. To achieve this, we alter the frequency of the vibratory stimuli displayed to the user according to the velocity of the user's finger as suggested in Maeno et al. [11]. This enables the user to feel same number of haptic bumps on the surface if she/he moves her/his finger with a low or high velocity on the surface.

In order to generate a wide range of haptic bumps on the glass surface, we use the concept of amplitude modulation. In communication systems, for example, if transmission requires a particular frequency, the information to be transmitted is embedded in a carrier signal (high frequency signal) matching the desired low frequency. This concept has already been utilized in haptics community to display vibrotactile stimuli to a user. Brown et al. [12] utilized vibrotactile actuators to modulate low frequency sinusoidal waves at 20, 30, 40, and 50 Hz with a high frequency sinusoidal wave at 250 Hz to investigate the perception of roughness and rhythm through vibration. The experiments conducted with 18 subjects showed that the subjects were successful in differentiating roughness and rhythm with success rates of 80% and 93%, respectively. Maeno et al. [11] utilized an ultrasonic frequency as the carrier signal to display low frequency tactile textures.

Again using amplitude modulation, Ahmaniemi et al. [13] successfully displayed virtual textures through a vibrotactile actuator. Park and Choi [14] investigated the perceptual dimensions of amplitude-modulated vibrotactile stimuli displayed by a voice-

coil actuator. A sinusoidal signal at 150 Hz was modulated by seven low frequency sinusoidal signals varying from 1-80 Hz. The analysis showed that the pulse-like sensation was observed at low modulation frequencies of 1–10 Hz.

In all of the above studies, the vibrations are displayed by a vibrotactile actuator held by a user. In our implementation, the vibrations of the plate at first resonance frequency are convolved with the low frequency waves to display vibrotactile haptic bumps to the finger of a user moving on the glass plate. Hence, our vibrotactile stimuli have components in both time and spatial domains. In order to display haptic bumps on the surface of the plate, we, for example, first convolve a low frequency sinusoidal signal with the first resonance frequency of the plate to obtain a modulated signal of the form

$$y(t) = A \sin(2\pi f_d t) \sin(2\pi f_c t) \tag{16}$$

where, A is the peak amplitude of the modulated signal, f_d is the frequency of the desired signal and f_c is the frequency of the carrier signal (i.e. the first resonance mode of the plate, $f_1 = 158$ Hz). Now, if we substitute v/λ for f_d, then the sine wave equation becomes

$$y(t) = A \sin\left(2\pi \frac{x(t)}{\lambda}\right) \sin(2\pi f_c t) \tag{17}$$

where, $x(t)$ is the finger position and λ is the wave length of the desired low frequency signal, which, in fact, determines the number of bumps displayed to the user. The finger position is acquired by the infrared frame in our set-up (see Figure 2.1 and Figure 2.4(a)).

In our implementation, we only consider the positive parts of the modulated signal (i.e. unipolar signal), $y(t)$, to display haptic bumps on the surface of the plate. In addition to using a sine wave as the modulated signal, we also utilize square and sawtooth waves and alter the wavelength and duty cycle of a wave to create haptic bumps in different ridge and groove widths. Since wavelength determines the number of bumps displayed on the surface and it is easier to understand for the reader, we use the term number of bumps (*NB*) instead

of wavelength in the text. Hence, there are four parameters that can be adjusted by the developer to generate various haptic bumps on the surface in our approach:

    n   : Wave form (determines the surface shape of the bumps)

    NB : Number of bumps (determines the spatial frequency of the bumps)

    DC : Duty cycle (determines the ratio of on-time/total time of each bump)

    A   : Peak amplitude (determines the peak amplitude of the bumps)

Chapter 4

HUMAN EXPERIMENTS

4.1 Participants

We have conducted an experimental study with 10 human subjects to investigate the perceptual effects of haptic bump on the subjects. Six men and four women participated in the experiment. The ages of the participants were varied between 23 and 28 (average = 26.2 ± 1.5). All of them were right-handed and used their index finger to explore the surface.

4.2 Stimuli

Using the proposed approach and the parameters defined in the previous section, various haptic bumps were generated on the glass surface for testing. 81 different haptic bumps are tested by choosing the parameters as $n = \{$sine, square, sawtooth$\} \times NB = \{2, 6, 18\} \times DC = \{0.2, 0.5, 0.8\} \times A = \{0.5, 4, 7.5$ Volts$\}$. The voltage amplitudes were amplified by 50 before transmitted to the piezo patches. For those voltage amplitudes, the corresponding out-of-plane displacements at the center point of the glass plate (point A in Figure 2.4(b) are $\{15, 120, 225\ \mu m\}$. The intervals between the values in parameter sets were selected by considering the just noticeable difference (JND) of human vibrotactile perception. Choi and Kuchenbecker [20] review the literature and suggest at least 20-30 % difference in frequency and amplitude for robust discrimination between vibrotactile

stimuli in practical settings. Duty cycle and the number of bumps are the two parameters that affect the bump width and space between the bumps, which corresponds to ridge width and groove width in the literature. The corresponding ridge width and groove width values for the bumps displayed in our experiments are presented in Table 4.1.

Table 4.1: The ridge width (RW) and the groove width (GW) of the bumps used in our experiments

DC / NB	0.2		0.5		0.8	
	RW (mm)	GW (mm)	RW (mm)	GW (mm)	RW (mm)	GW (mm)
2	10	40	25	25	40	10
6	3.33	13.33	8.33	8.33	13.33	3.33
18	1.11	4.44	2.78	2.78	4.44	1.11

While creating the haptic bumps, one parameter is changed each time while keeping the others constant. Each stimulus was displayed 4 times to the subjects. Hence, the total number of trials for each subject was 324 (81 haptic stimuli $\times$ 4 repetitions), which was displayed in random order while the order was same for all the subjects. The haptic bumps displayed to the subjects are shown in Figure 4.1 for unit amplitude.

The software for displaying the haptic stimuli was developed in MATLAB/Simulink using the Real Time Windows Target (see Appendix B). Two desktop computers and two DAQ cards are used during the experiments. The first computer is used to acquire the finger position and this data is sent to the first DAQ card's analog output channel. This output channel is connected to the second DAQ card's input channel which is connected to the second computer. The position data is then processed in the second computer running MATLAB/Simulink to generate the desired haptic stimuli, which is transmitted to the piezo patches using the analog output channel of the second DAQ card.
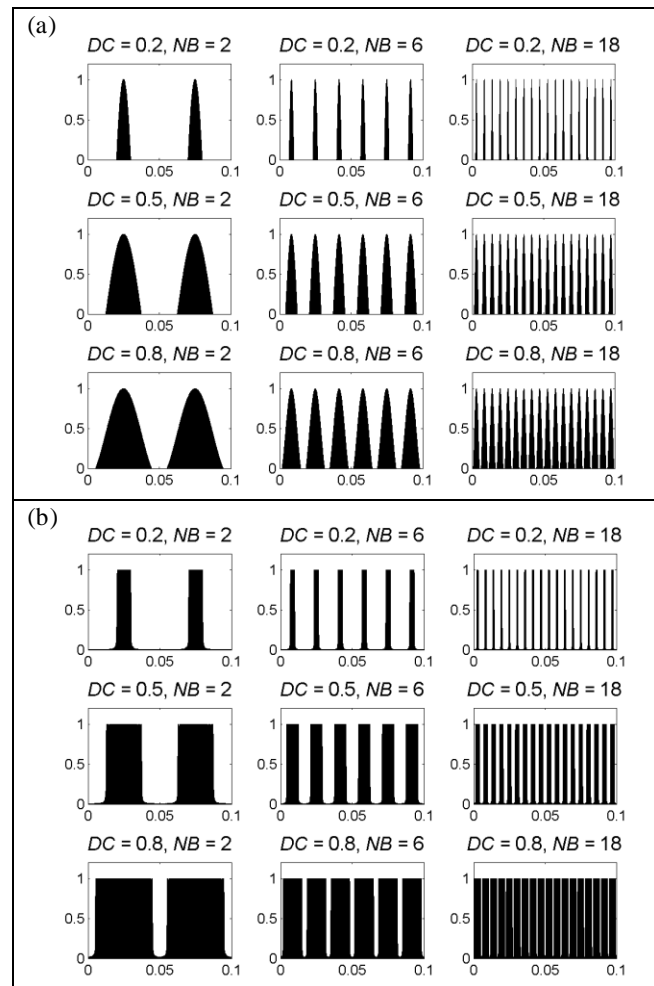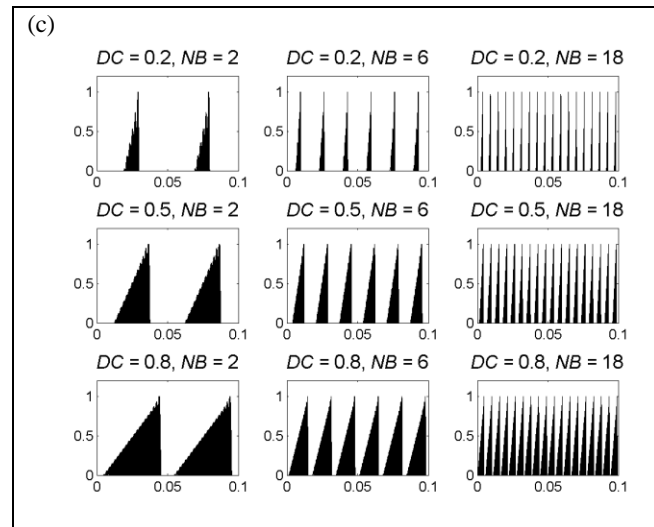
Figure 4.1: Haptic bumps displayed to the subjects (for unit amplitude): (a) sinusoidal, (b) square, and (c) sawtooth.

4.3 Experimental Procedure

The subjects were instructed to sit on a chair in front on the setup and move their index finger back and forth in the horizontal direction on the touch screen to differentiate the haptic stimuli (Figure 4.3). They are allowed to move their finger only in 10×4 cm rectangular region on the touch screen constraint by a black cartoon board. Lederman [21] suggests that lateral motion is the most optimal procedure for exploring surface details. The subjects explored the surface for 15 seconds by moving their index finger horizontally back and forth on the touch screen in the rectangular region of 10×4 cm. Note that the displacement amplitude varies on the glass plate along the horizontal axis (x−axis in Figure 2.4(b)) for its first mode (see Figure 4.2). To compensate for those changes, we modify the voltage applied to the piezo actuators on the fly with respect to the finger position of the user on the horizontal axis. Using this approach, we increase all the displacements along

the horizontal axis to the max value (i.e. the value at the center point). For this purpose, we use a simple look-up table and a polynomial interpolation function. The points shown in the plot corresponds to the LDV measurements with spacing of 2.5 cm.
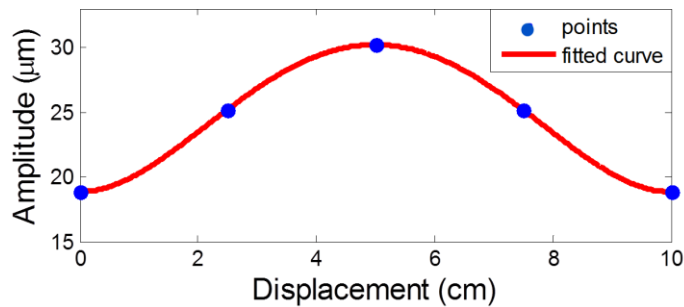
Figure 4.2: The change in out-of-plane displacement amplitudes along the horizontal axis within the rectangular region of 10×4 cm (refer to Figure 4.3).

During the experiments, the subjects were allowed to replay the haptic stimuli once more by pressing the replay button. To reduce tiring of the subjects, a large size soft pad was placed under their wrist. The subjects were asked to wear headphones, playing white noise, to prevent the acoustic noise affecting their haptic perception. Before starting the experiment, the subjects were given instructions about the experiment and presented a training session introducing the different combinations of the haptic bumps (note that the subjects were not explicitly told that they would feel bumps on the surface) (see Appendix C). It took about 2.5 hours for each subject to complete the experiment including the training session. The experiments were performed on two consecutive days; the first day included a training session and then two sets of stimuli presented to the subjects and in the second day, the last two sets of stimuli presented to the subjects.

In each trial, the subjects were asked to differentiate what they felt on the glass surface based on the following adjective pairs (the definition of these adjective pairs were introduced to the subjects prior to the experiments)

- *smooth* (an even surface that is free from irregularities) versus *rough* (an uneven surface with irregularities on it)
- *flat* (a surface with no bumps) versus *bumpy* (a surface with "countable" bumps).

These adjectives were selected based on the earlier studies in literature on human haptic texture perception (Hollins et al. [22], [23]), which suggests that rough/smooth and flat/bumpy adjectives receive similar ratings in roughness perception. A Likert scale of 1-7 is used to rate the perceptual feelings of the subjects. After each trial, the subjects used a digitizing pen held by the non-dominant hand to enter the magnitude of their perception using a simple graphical user interface shown on the computer screen (see Figure 4.3).

Figure 4.3: The experimental setup and the graphical interface used for the human experiments.

Chapter 5

RESULTS

Each adjective pair (smooth/rough, flat/bumpy) was analyzed separately with 4-way ANOVA. The factors in the analysis were the a) wave form, b) wave length, c) duty cycle, and d) peak amplitude.

The results of ANOVA show that the wave form, wave length, duty cycle, and peak amplitude have significant effects on the haptic perception of roughness. Bonferroni corrected paired t-tests showed that the perception of roughness has increased as the spatial frequency, duty cycle, and peak amplitude of the bumps has increased (see the box plots in Figure 5.1(a)). The ones marked with stars shows the couples which are not statistically significant. Note that all differences between the groups in Figure 5.1(a) were statistically highly significant ($p < 0.001$). The difference between the waveforms was also highly significant and the subjects perceived the square wave as the roughest while the sawtooth was perceived as the smoothest among 3 waveforms.

Although the ANOVA results also show that the wave form, wave length, duty cycle, and peak amplitude have significant effects on the haptic perception of bumpiness, the ratings were only parallel for the peak amplitude. Again, the subjects perceived the surface bumpier as the peak amplitude has increased, but the change in their perception did not follow a monotonically increasing trend with increasing spatial frequency or duty cycle (Figure 5.1(b)). In terms of the waveforms, only the sinusoidal wave was perceived significantly bumpier than the sawtooth wave.

(a)

(b)
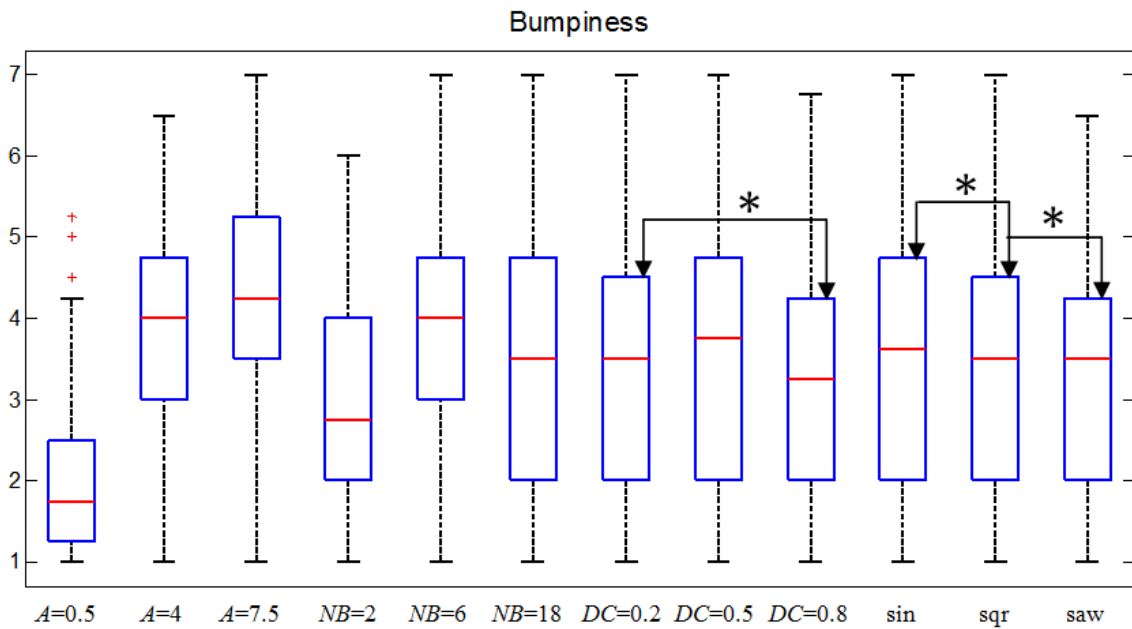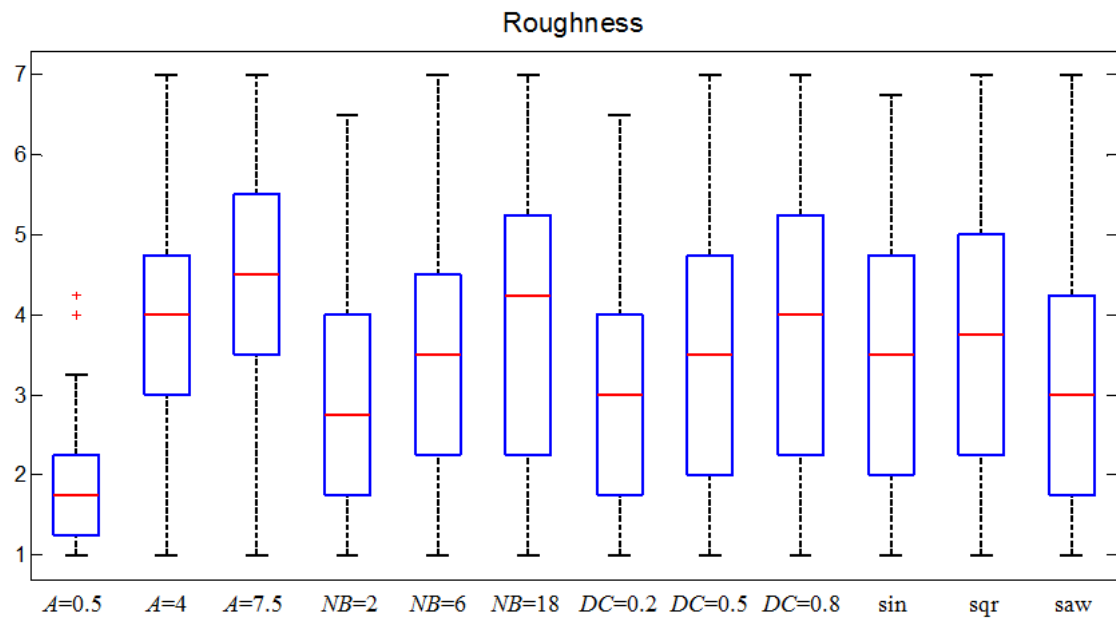
Figure 5.1: The box-plots for roughness (a) and bumpiness perception (b).

Chapter 6

DISCUSSION

Although the roughness is known to be one of the most important dimensions in haptic perception of textures, it is still difficult to say which characteristics of the texture most contribute to the perception of roughness. It has been suggested that peak amplitude, wavelength (spatial frequency), friction, and spacing between the surface features such as dots, bumps, and ridges play critical role [24]. It is important to note here that the bump textures in our study are displayed to the subjects in the form of vibrotactile stimuli and not in the form of topological height variations on the surface. Hence, the haptic perception of bumps displayed to the subjects in our study is also related to the human vibrotactile perception and we compare our results with those in both domains for the sake of completeness.

Human haptic perception of roughness has been investigated extensively through texture perception studies. Hollins et al. [22] used multi dimensional scaling (MDS) to investigate the dimensions of human haptic perception of textures. They identified the rough/smooth and hard/soft as the perceptual dimensions that are perpendicular to each other. The ratings for flat/bumpy were observed to be similar to those of smooth/rough and sticky/slippery were not found to be independent of the other dimensions. These findings were further confirmed by Hollins et al. [23] and Yoshioka et al. [25] in later studies. Based on these findings, we used the rough/smooth and flat/bumpy adjectives in our study of roughness perception. The sticky/slippery adjective was not preferred in our subjective ratings since our system does not effectively change the surface friction as in the case of ultrasonic piezo actuation [6], [7], [8].   The ratings for rough/smooth and flat/bumpy

showed the similar trend only for the peak amplitude and not for the spatial frequency, duty cycle, and wave form. In our instructions to the subjects, we defined the bumpy surface as the one with "countable" bumps. As the spatial frequency and duty cycle of the bumps are increased, the gap between the bumps (i.e. inter-element spacing/groove width) is reduced (see Table 4.1) and it became more difficult to count the number of bumps on the surface. For example, when NB = 18 (i.e. 18 bumps are displayed in 10 cm), it felt like a continuous vibration with varying peak amplitude rather than individual bumps. Hence, the subjects perceived this as a rough surface but not a bumpy surface since the bumps are not countable.

Effect of Peak Amplitude (Bump Height): Our results also show that the perceived roughness and bumpiness increase with the peak amplitude of the vibrations. In this regard, our results are in good agreement with the earlier studies. The studies on human haptic perception of textures and gratings, performed in real and virtual [26] worlds, strongly suggest that the perceived roughness increase with the height of the surface details. Rantala et al. [27] used a single piezo actuator placed under a touch screen to display six-dot Braille characters via vibration. The raised dots were displayed by higher amplitude vibratory bumps while the lower ones were represented with less powerful vibrations to indicate the blanks. The results of the experiments performed with 5 blind subjects show that subjects could successfully differentiate the amplitude difference and read the individual characters with an accuracy of 97% after 3 sessions.

Effect of Wavelength (Spatial Frequency) and Duty Cycle: In our system, increasing the number of bumps while fixing the duty cycle or increasing the duty cycle while fixing the number of bumps reduces the inter-element space between the bumps. Our results are not in agreement with the earlier studies. We found that the perceived roughness increases with the increasing (decreasing) spatial frequency (inter-element spacing) of the bumps and their duty cycle. In terms of inter-element spacing between the surface features,

Lederman and Taylor [28] observed that the spacing between the ridges of macrotextures (textures having inter-element spacing larger than approximately 0.2 mm) has a greater effect on perceived roughness than the ridge width. This observation has been supported by other studies later [29] suggesting that the perceived roughness increases monotonically with the spacing, but decreases modestly with the ridge width. On the other hand, further increasing the spacing between the surface features (more than 3.5 mm) causes the subjects perceive the surface as smooth rather than rough [30]. Ahmaniemi et al. [13] used a simple motion sensor, a single vibration actuator, and the amplitude modulation approach to display virtual textures (in the form of vibratory stimuli as in our study) and the results of the experimental study conducted with 16 subjects showed that ridge width and spatial density had significant on perceived roughness and flatness. The subjects perceived the vibrotactile textures rougher and bumpier as the ridge width and the spatial frequency are decreased.

The discrepancy between our findings and the earlier studies on haptic texture perception can be attributed to several factors. One factor is related to the differentiation of the micro versus macro textures. With respect to the definition given by Lederman [28], all textures in our experiments are macrotextures. Hollins et al. [31] and Klatzky and Lederman [32] state that the perception of microtextures is mainly achieved by vibratory cues through Pacinian Corpscule mechanoreceptors while that of the macrotextures is achieved by spatial cues through pressure change and finger deformation. However, in our study, the haptic stimulus is mainly perceived through the vibrotactile channel via Pacinian Corpscule mechanoreceptors and the effect of pressure change and finger deformation on this perception is less significant. Another factor for the discrepancy could be related to the definition of terms "rough" and "bumpy. For example, in texture perception studies conducted with a haptic device in virtual environments, Klatzky and Lederman [33] instructed their subjects to judge roughness by imagining that they were in a car moving

over a bumpy road. Note that we defined the bumpy surface as the one with "countable" number of bumps so that the subjects could differentiate it from a rough surface, which was defined as an uneven surface with irregularities on it.

Effect of Waveform: Our results show that the subjects perceived the square wave as the roughest while the sawtooth was perceived as the smoothest among 3 waveforms. The differences were not very distinguishable in perception of bumpiness. Although the bumpiness perception of the sawtooth wave was the lowest, only the sinusoidal wave was perceived significantly bumpier than the sawtooth wave. Hence, in general, it can be concluded that the square and sinusoidal waves are better in creating a perception of roughness and bumpiness than the sawtooth wave.

The number of research studies in this area is limited and this topic requires further investigation. The existing studies partially support our findings. Cholewiak et al. [34] conducted human experiments in virtual environments using a haptic device to investigate the amplitude detection thresholds for virtual haptic gratings (bumps) in the form of sinusoidal and square waves. The results showed that the detection threshold for the square wave gratings was lower than that of the sinusoidal gratings. Kocsis et al. [35] conducted discrimination experiments with real and virtual sinusoidal and triangular textured surface gratings. All gratings had a wave length of 2.5 mm and the height (wave amplitude) varying from 55-70 µm. The results showed that the discrimination thresholds did not differ significantly between sinusoidal and triangular gratings. MacLean and Enriquez [36] used a knob connected to the shaft of a motor to display tactile stimuli (called haptic icons) by varying the frequency and magnitude of sinusoidal, triangular, square, triangle and sawtooth waves. They conducted experiments with 8 subjects and 36 different haptic icons. The experiments showed the dominance of sinusoidal wave over square/sawtooth wave in transmitting haptic information.

Effect of RMS Value on the Roughness Perception: As explained before, the results of our system are not in agreement with the earlier studies in terms of the effect of wavelength and duty cycle on the roughness perception. But it is important to mention that, in the earlier studies, the relation between the groove/ridge width and roughness perception was investigated using physical (real) surfaces like aluminum plates with actual ridges and grooves. Since our stimuli are presented in the form of vibrotactile signals, it is more meaningful to consider the effective vibration amplitude in the analysis rather than the ridge and groove widths. For this reason, we calculated the RMS amplitudes of the vibratory signals, which are affected by the shape, duty cycle of the signals, but not the number of bumps.

For a discrete set of n amplitudes values such as $\{x_1, x_2, \ldots, x_n\}$, RMS is calculated as

$$x_{RMS} = \sqrt{\frac{1}{n}(x_1^2 + x_2^2 + \cdots + x_n^2)} \tag{18}$$

Using the above expression, the RMS amplitudes of all of our stimuli were calculated. Since the RMS amplitude is calculated over one period for a periodic signal, it is independent of the number of bumps presented to the user. Hence, we ended up with 27 different RMS amplitudes for 81 stimuli. The RMS amplitudes and the corresponding roughness perceived by the subjects are given in Table 6.1 and Table 6.2, and depicted in Figure 6.1.

By looking at Table 6.1 it can be concluded that the RMS amplitudes increase as the peak amplitude and duty cycle increase. Also, the RMS amplitudes are the highest for square signals and the lowest for sawtooth signals. If these results are compared with the average roughness values shown in Table 6.2, it is clearly observed that there is a direct relation between the RMS amplitudes and roughness perception. According to these results, it is expected that subjects should have similar perception of roughness for two different vibratory stimuli having similar RMS amplitudes. Figure 6.1 strongly supports this notion. For example, for the blue triangle and the yellow circle shown in Figure 6.1

with the RMS amplitudes of 0.99 V and 1 V respectively, the roughness perceived by the subjects is nearly identical. Note that the blue triangle represents a sawtooth signal with peak amplitude of 4 V and duty cycle of 0.8 and the yellow circle represents a sine signal with peak amplitude of 4V and duty cycle of 0.5. Similarly, for the green and red triangles with the RMS amplitudes of 0.8 V and 0.83 V respectively, the roughness perceived by the subjects is again the same (Note that the green triangle represents a sawtooth signal with a peak amplitude of 4 V and duty cycle of 0.5 and the red triangle represent a sawtooth signal with a peak amplitude of 7.5 V and duty cycle of 0.2).

Table 6.1: The RMS amplitudes of the stimuli (in Volts)

	A = 0.5 V			A = 4 V			A = 7.5 V		
	Sin	Sqr	Saw	Sin	Sqr	Saw	Sin	Sqr	Saw
DC = 0.2	0.08	0.11	0.06	0.65	0.89	0.44	1.23	1.66	0.83
DC = 0.5	0.13	0.18	0.10	1	1.41	0.80	1.88	2.64	1.51
DC = 0.8	0.15	0.22	0.12	1.18	1.79	0.99	2.21	3.35	1.85

Table 6.2: The roughness perceived by the subjects based on the Likert scale of 1-7 (the average values and the standard deviations)

	A = 0.5 V			A = 4 V			A = 7.5 V		
	Sin	Sqr	Saw	Sin	Sqr	Saw	Sin	Sqr	Saw
DC = 0.2	2.04±0.77	1.93±0.86	1.42±0.41	3.77±1.16	3.46±1.01	3.04±0.97	3.92±1.24	3.95±1.15	3.68±1.22
DC = 0.5	1.84±0.63	1.89±0.67	1.63±0.59	3.96±1.15	4.30±1.18	3.73±0.89	4.34±1.25	4.91±1.27	4.27±1.22
DC = 0.8	1.82±0.59	1.95±0.61	1.80±0.64	4.40±1.21	4.82±1.14	3.98±1.13	5.03±1.24	5.15±1.38	4.68±1.06

The relation between the peak amplitude, duty cycle, wave form and the roughness perception can be explained with respect to the RMS amplitudes. But, this notion cannot be extended to explain the relation between the number of bumps and the roughness

perception, since the RMS amplitude of the stimulus used in our experiments is not affected by the change in the number of bumps. To investigate the effect of number of bumps on the roughness perception, we regrouped the experimental data such that the RMS amplitude, the duty cycle and the peak amplitude were fixated for each wave form. Figure 6.2 shows the relation between the number of bumps and roughness perception for three different wave forms. As shown in this figure, the perception of roughness clearly increases with the increase in the number of bumps for the peak amplitudes of 4 V and 7.5 V, but stays almost constant for the peak amplitudes of 0.5 V.
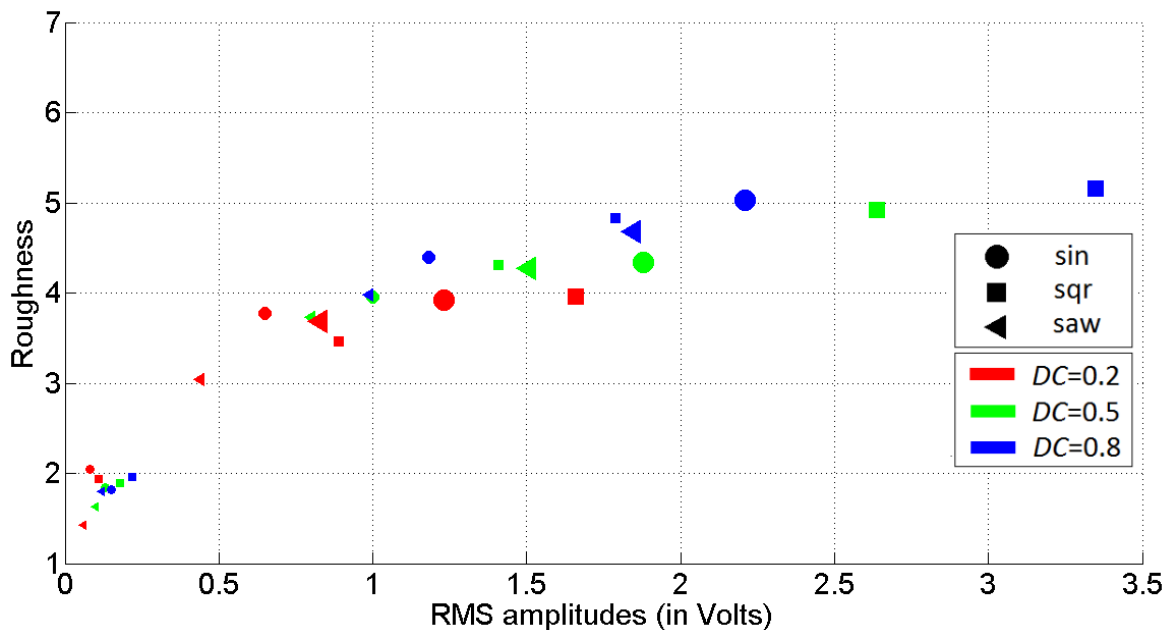
Figure 6.1: The RMS amplitudes (in Volts) vs perceived roughness graph for 27 different stimuli: The marker shapes (circle, square, triangle) stand for the wave form (sin, sqr, saw), the marker sizes (small, medium, large) stand for the peak amplitudes (A = 0.5 V, 4V, 7.5 V), and the marker colors (red, green, blue) stand for the duty cycle (DC = 0.2, 0.5, 0.8). Small marker sized stimuli have peak amplitude of 0.5, medium sized stimuli have peak amplitude of 4 and large sized stimuli have peak amplitude of 7.5.
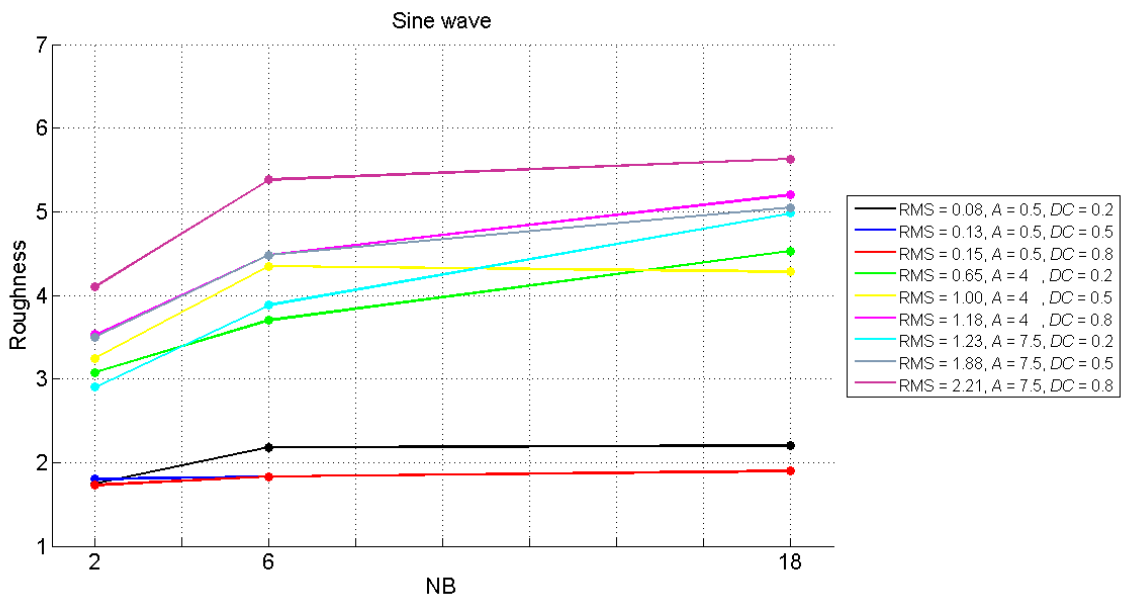
(a)
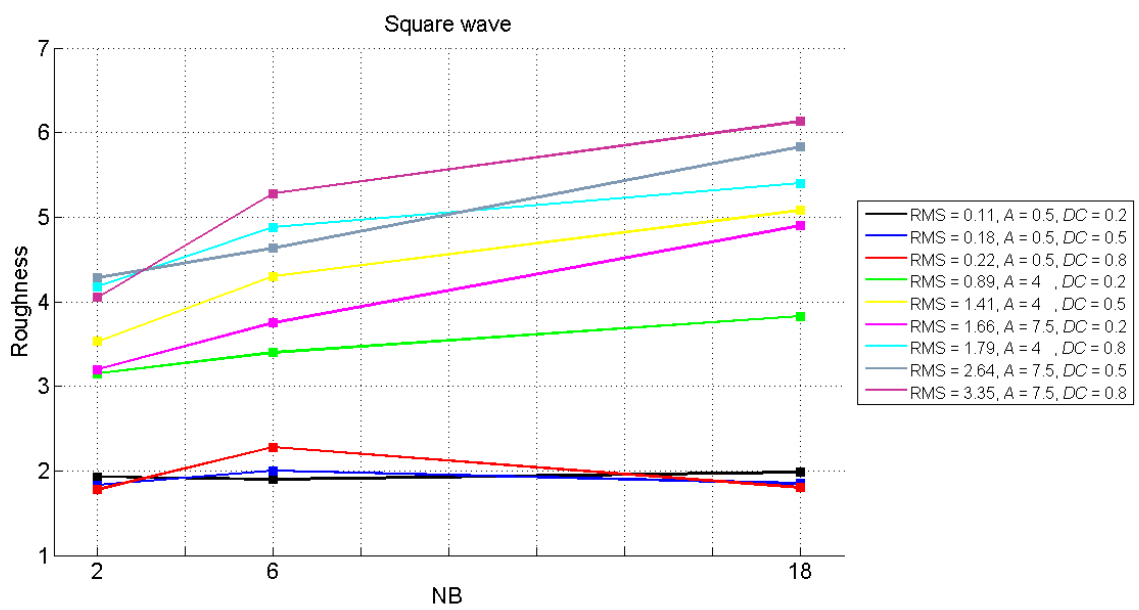
(b)
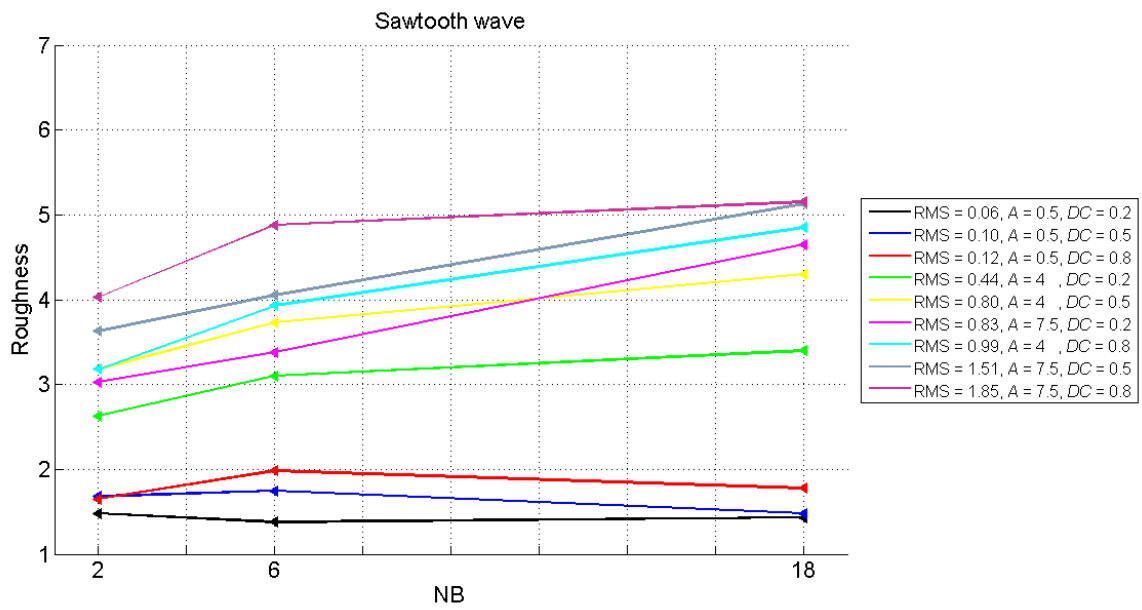
(c)

Figure 6.2: The variation in roughness perception as a function of number of bumps for (a)sine, (b)square and (c)sawtooth waves.

Chapter 7

CONCLUSION

The touch screens replace the mechanical buttons on mobile devices, touch pads, tablet PCs and other displays. While the screens available in the market today are sensitive to touch inputs and gestures, they do not enable the user to feel any programmable resistive forces as her/his finger moves on its surface. However, it is desirable to display some of the information through haptic channel in mobile devices, touch pads, tablet PCs and other interactive displays in order to alleviate the perceptual and cognitive load of the user since our visual and auditory channels are already highly overloaded. Moreover, haptic feedback is more personal and intimate than visual and auditory feedback and hence can enrich the user experience and perception of the interaction. We anticipate that the use of haptic feedback as an additional information channel in interactive displays will result in a new interaction paradigm, and enable novel applications in games, entertainment, education, internet-based business, and many more.

The goal of our study was to produce programmable vibrations on the surface of a touch screen via piezo actuators attached to its surface. Most of the systems conveying programmable vibrotactile stimuli today either display relatively simple haptic effects such as button clicks, contact/collision events or are passive systems (e.g. hand held vibrotactile actuators or vibrotactile actuators placed to body surface). Displaying haptic effects on a touch screen via vibrotactile cues during an active haptic exploration is more challenging. Currently, there are no established methods on a) how many piezo patches must be used and b) how they must be attached to a touch screen to generate the desired haptic effects on a surface with maximum displacement and minimum power. Since the piezo patches

cannot be easily detached from a touch screen once they are glued to its surface, it is more convenient to construct our designs in a simulation environment and test it using a finite element package. One of the challenges in the design is the selection of appropriate boundary conditions and the piezo configurations on the screen for achieving optimum performance within the limits of human haptic perception. To investigate the design trade-offs, we developed a finite element model of the screen and four piezo actuators attached to its surface in ABAQUS. A boundary condition clamping the glass plate from short edges was selected to cover larger range frequencies within the limits of human vibrotactile perception. After selecting the appropriate boundary condition for the screen based on the range of vibration frequencies that are detectable by a human user, the optimum configuration for the piezo patches is determined by maximizing the vibration amplitude of the screen. The results of our finite element analysis showed that the piezo patches must be placed close to the boundary edges and not the free edges [15].

After the design of the touch screen, we conducted experiments with 10 subjects to investigate the human active haptic perception of roughness by displaying virtual bump textures on our touch screen. To display various haptic bumps in different shape and size, we used sinusoidal, square, and sawtooth pulse waves and varied their amplitude, spatial frequency, and duty cycle. Results of our experimental study show that perception of roughness and bumpiness exhibits similar behavior to the amplitude change, it increases as the amplitude of the vibrations increases. On the other hand, effects of wavelength and duty cycle do not show a parallel behavior for these two adjectives. Roughness perception increases as the spatial frequency or duty cycle increases whereas bumpiness perception shows a parabolic behavior with increasing duty cycle. Another point is that square wave perceived as the roughest while the sine wave perceived as the bumpiest in our experiments. We also observed that there is a close relation between the RMS amplitudes of the signals and the perceived roughness. Based on the user study, vibratory stimuli that

have close RMS amplitudes are perceived to be similar in roughness. Also, the perceived roughness increases as the RMS amplitude increases.

One improvement to our current design may involve adding piezo actuators that are capable of vibrating at ultrasonic frequencies. Then, it might be possible to create air gap between the finger and the vibrating surface as suggested in [6], [7], [8]. As a result, slippery/sticky haptic effect can be created on the touch screen. Another potential extension might be investigating the effect of signal polarity on the haptic perception. In the current design, only positive unipolar signals are presented to the user, while the effect of negative or bipolar signals on the haptic perception has not been investigated as done in [1]. Also in the current setup, haptic effects change only in the horizontal direction (x-axis in Figure 2.4(b)). These effects can be enriched further by considering the vertical direction (y-axis in Figure 2.4(b)). By considering both dimensions on the plate, a rich set of textured surfaces can be created by altering the frequency, phase and, amplitude of the desired signals in x and y-axes as suggested in Basdogan et al. [37] for haptic texture rendering. One final possible study might be on eliminating the acoustic noise created by the piezo patches.

BIBLIOGRAPHY

[1] K.A. Kaczmarek, K. Nammi, A.K. Agarwal, M.E. Tyler, S.J. Haase, and D.J. Beebe, "Polarity Effect in Electrovibration for Tactile Display," *IEEE Trans. Biomedical Engineering*, vol. 53, no. 10, 2006, pp. 2047-54.

[2] A. Yamamoto, S. Nagasawa, H. Yamamoto, and T. Higuchi, "Electrostatic Tactile Display with Thin Film Slider and Its Application to Tactile Telepresentation Systems," *IEEE Trans.Visualization and Computer Graphics*, vol. 12, no. 2, 2006, pp. 168-177.

[3] O. Bau, I. Poupyrev, A. Israr, and C. Harrison, "TeslaTouch: Electrovibration for Touch Surfaces," *Proc. 23rd ACM Symp. User Interface Software and Technology,* 2010, pp.283-292.

[4] M. Fukumoto and T. Sugimura, "Active Click: Tactile Feedback for Touch Panels," *Proc. Conf. Human Factors in Computing Systems*, ACM, 2001, pp. 121-122.

[5] S. Kim and J.C. Kim, "Vibrotactile Rendering for a Traveling Vibrotactile Wave Based on a Haptic Processor," *IEEE Trans. Haptics*, vol. 5, no. 1, 2012, pp. 14-20.

[6] M. Biet, G. Casiez, F. Giraud, and B. Lemaire-Semail, "Discrimination of Virtual Square Gratings by Dynamic Touch on Friction Based Tactile Displays," *Proc. Symp. Haptic Interfaces for Virtual Environment and Teleoperator Systems*, 2008, pp. 41-48.

[7] F. Giraud, M. Amberg, and B. Lemaire-Semail, "Design and Control of a Haptic Knob," *Sensors and Actuators A: Physical*, vol. 196, 2013, pp. 78-85.

[8] L. Winfield, J. Glassmire, J.E. Colgate, and M.Peshkin, "T-PaD: Tactile Pattern Display through Variable Friction Reduction," *Proc. 2nd Joint EuroHaptics Conf. and*

Symp. Haptic Interfaces for Virtual Environment and Teleoperator Systems, IEEE, 2007, pp. 421-426.

[9] E.C. Chubb, J.E. Colgate, and M.A. Peshkin, "ShiverPad: A Device Capable of Controlling Shear Force on a Bare Finger," *Proc. 3rd Joint EuroHaptics Conf. and Symp. Haptic Interfaces for Virtual Environment and Teleoperator Systems*, vol. 3, no. 3, 2009, pp. 18-23.

[10] X. Dai, J.E. Colgate, and M.A. Peshkin, "LateralPaD: A Surface-Haptic Device That Produces Lateral Forces on A Bare Finger," *Proc. IEEE Haptics Symp.,* 2012, pp. 7-14.

[11] T. Maeno, K. Otokawa, and M. Konyo, "Tactile Display of Surface Texture by use of Ultrasonic Vibration," *Proc. IEEE Ultrasonic Symp.*, 2006, pp. 62-65.

[12] L.M. Brown, S.A. Brewster, and H.C. Purchase, "A First Investigation into the Effectiveness of Tactons," *Proc. IEEE World Haptics Conf.* (WHC 05), 2005, pp. 167-176.

[13] T. Ahmaniemi, J. Marila, and V. Lantz, "Design of Dynamic Vibrotactile Textures," *IEEE Trans. Haptics*, vol. 3, no. 4, 2010, pp. 245-256.

[14] G. Park and S. Choi, "Perceptual Space of Amplitude-Modulated Vibrotactile Stimuli," *Proc. IEEE World Haptics Conf.* (WHC 11), 2011, pp. 59-64.

[15] B. Baylan, U. Aridogan, and C. Basdogan, "Finite Element Modeling of a Vibrating Touch Screen Actuated by Piezo Patches for Haptic Feedback," *Proc. EuroHaptics*, 2012, pp. 47–57.

[16] L.A. Jones and N.B. Sarter, "Tactile Displays: Guidance for Their Design and Application," *Human Factors: The Journal of the Human Factors and Ergonomics Soc.*, vol. 50, 2008, pp. 90–111.

[17] "IEEE Standard on Piezoelectricity," *ANSI/IEEE Std. 176-1987*, IEEE, 1988.

[18] *Piezoelectricity*, J. Emery, 1997.

[19] V. Piefort, "Finite Element Modeling of Piezoelectric Active Structures," PhD thesis, Faculty of Applied Sciences, Universit'e Libre de Bruxelles, Belgium, 2001.

[20] S. Choi and K.J. Kuchenbecker, "Vibrotactile Display: Perception, Technology, and Applications," *Proc. IEEE*, vol. 101, no. 9, 2013, pp. 2093-2104.

[21] S.J. Lederman, "Tactile roughness of grooved surfaces: The touching process and effects of macro- and microsurface structure," *Perception & Psychophysics*, vol. 16, no. 2, 1974, pp. 395-395.

[22] M. Hollins, R. Faldowski, S. Rao, and F. Young, "Perceptual dimensions of tactile surface texture: A multidimensional scaling analysis," *Perception & Psychophysics*, vol. 54, no. 6, 1993, pp. 697–705.

[23] M. Hollins, S. Bensmaïa, K. Karlof, and F. Young, "Individual differences in perceptual space for tactile textures: Evidence from multidimensional scaling," *Perception & Psychophysics*, vol. 62, no. 8, 2000, pp. 1534–1544.

[24] W.M. Bergmann Tiest, "Tactual perception of material properties," *Vision Research*, vol. 50, no. 24, 2010, pp. 2775-2782.

[25] T. Yoshioka, S.J. Bensmaïa, J.C. Craig, and S.S. Hsiao, "Texture perception through direct and indirect touch: An analysis of perceptual space for tactile textures in two modes of exploration," *Somatosensory and Motor Research*, vol. 24, no. 1-2, 2007, pp. 53–70.

[26] R.L. Klatzky and S.J. Lederman, "The Perceived Roughness of Resistive Virtual Textures: I. Rendering by a Force-Feedback Mouse," *ACM Trans. Applied Perception*, vol. 3, no. 1, 2006, pp. 1-14.

[27] J. Rantala, R. Raisamo, J. Lylykangas, V. Surakka, J. Raisamo, K. Salminen, T. Pakkanen, and A. Hippula, "Methods for Presenting Braille Characters on a Mobile Device with a Touchscreen and Tactile Feedback," *IEEE Trans. Haptics*, vol. 2, no. 1, 2009, pp. 28-39.

[28] S.J. Lederman and M.M. Taylor, "Fingertip force, surface geometry, and the perception of roughness by active touch," *Perception & Psychophysics*, vol. 12, no. 5, 1972, pp. 401-408.

[29] C.J. Cascio and K. Sathian, "Temporal Cues Contribute to Tactile Perception of Roughness," *Journal of Neuroscience*, vol. 21, no. 14, 2001, pp.5289–5296.

[30] R.L. Klatzky, S.J. Lederman, C. Hamilton, M. Grindley, and R.H. Swendsen, "Feeling textures through a probe: Effects of probe and surface geometry and exploratory factors," *Perception & Psychophysics*, vol. 65, no. 4, 2003, pp. 613–631.

[31] M. Hollins, S.J. Bensmaïa, and S. Washburn, "Vibrotactile adaptation impairs discrimination of fine, but not coarse, textures," *Somatosensory and Motor Research*, vol. 18, no. 4, 2001, pp. 253-262.

[32] R.L. Klatzky and S. Lederman, "Multisensory texture perception," *Multisensory Object Perception in the Primate Brain*, 2010, pp. 211-230.

[33] S.J. Lederman, R.L. Klatzky, C. Tong, and C. Hamilton, "The Perceived Roughness of Resistive Virtual Textures: II. Fffects of Varying Viscosity with a Force-Feedback Device," *ACM Trans. Applied Perception*, vol. 3, no. 1, 2006, pp. 15–30.

[34] S.A. Cholewiak, K. Kim, H.Z. Tan, and B.D. Adelstein, "A Frequency-Domain Analysis of Haptic Gratings," *IEEE Trans. Haptics*, vol. 3, no. 1, 2010, pp. 3–14.

[35] M. Kocsis, S.A. Cholewiak, R.M. Traylor, B.D. Adelstein, E.D. Hirleman, and H.Z. Tan, "Discrimination of Real and Virtual Surfaces with Sinusoidal and Triangular Gratings Using the Fingertip and Stylus," *IEEE Trans. Haptics*, vol. 6, no. 2, 2013, pp. 181-192.

[36] K. MacLean and M. Enriquez, "Perceptual Design of Haptic Icons," *Proc. EuroHaptics*, 2003, pp. 351-363.

[37] C. Basdogan, C.-H. Ho and M.A. Srinivasan, "A Ray-Based Haptic Rendering Technique for Displaying Shape and Texture of 3D Objects in Virtual Environments," *Proc. ASME Dynamic Systems and Control Division*, 1997, vol. 61, pp. 77-84.

Appendix A

FINITE ELEMENT MODELING OF PIEZOELECTRIC PATCHES

Piezoelectric coupling equations for a piezoelectric element are as follows:

$$T = c \times S - e \times E \qquad\qquad \text{(A.1)}$$

$$D = e^T \times S + \varepsilon \times E \qquad\qquad \text{(A.2)}$$

The field variables T, S, E and D are defined in Table A.1.

Table A.1: Field variables

T : Stress vector	S : Strain vector	E : Electric field vector	D : Electrical displacement vector
$T = \begin{bmatrix} T_1 \\ T_2 \\ \vdots \\ T_6 \end{bmatrix}$	$S = \begin{bmatrix} S_1 \\ S_2 \\ \vdots \\ S_6 \end{bmatrix}$	$E = \begin{bmatrix} E_1 \\ E_2 \\ E_3 \end{bmatrix}$	$D = \begin{bmatrix} D_1 \\ D_2 \\ D_3 \end{bmatrix}$

For E and D, subscripts 1, 2 and 3 symbolizes the x, y and z axis respectively. Since strain and stress are symmetric tensors, the subscripts for them are re-labeled as given in the Table A.2. According to the table T_1, T_2, T_3 are the principal stresses and T_4, T_5, T_6 are the shear stresses.

Table A.2: Matrix notation

Subscript	Corresponding label
11	1
22	2
33	3
23 or 32	4
31 or 13	5
12 or 21	6

In the equations (A.1) and (A.2), there are three piezoelectric constants which are c, e and ε matrices. Because of the anisotropic nature of piezo ceramics, effects are dependent on

direction. For this reason, to link electrical and mechanical quantities double subscripts (e.g. e_{ij}) are introduced. The first subscript gives the direction of the excitation while the second one describes the direction of the system response. From Figure A.1, it is seen that the subscripts 1, 2, and 3 corresponds to x, y and z coordinates and 4, 5 and 6 corresponds to rotations (shear).
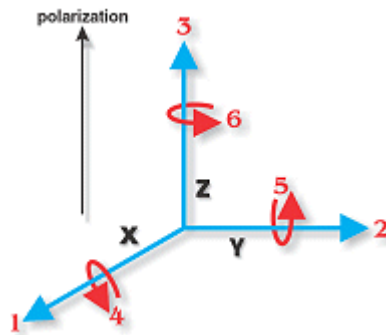

Figure A.1: Directions of forces affecting a piezoelectric element

For example, e_{15} applies when the electric field is along the x axis and the strain (deflection) is along the y axis, labeled as 5 in Figure A.1.

The definitions of the piezoelectric constant matrices are as explained below:

- c is the 6*6 elasticity matrix. Symmetry imposed by strain energy implies that this matrix is symmetric. Piezoelectric materials shows orthotropic behavior and a material is called orthotropic if it has three mutually perpendicular planes of symmetry. If the required transformations are applied about the x-y, y-z and x-z planes for this symmetry condition, only 12 nonzero variables are left. Also these transformations bring some relations about the constants of the matrix and finally it becomes:

$$
c = \begin{bmatrix}
c_{11} & c_{12} & c_{13} & 0 & 0 & 0 \\
c_{21} & c_{22} & c_{23} & 0 & 0 & 0 \\
c_{31} & c_{32} & c_{33}, & 0 & 0 & 0 \\
0 & 0 & 0 & c_{44} & 0 & 0 \\
0 & 0 & 0 & 0 & c_{55} & 0 \\
0 & 0 & 0 & 0 & 0 & c_{66}
\end{bmatrix}
$$

$$
= \begin{bmatrix}
c_{11} & c_{12} & c_{13} & 0 & 0 & 0 \\
c_{12} & c_{11} & c_{13} & 0 & 0 & 0 \\
c_{13} & c_{13} & c_{33}, & 0 & 0 & 0 \\
0 & 0 & 0 & c_{44} & 0 & 0 \\
0 & 0 & 0 & 0 & c_{44} & 0 \\
0 & 0 & 0 & 0 & 0 & 2(c_{11} - c_{12})
\end{bmatrix}
$$

- The matrix e is defined as the product of c and the transpose of d, $e=cd^{T}$

- d is a matrix containing 3*6 piezoelectric coefficients

On a macroscopic scale, three different transduction modes are possible:

i) In the thickness or d_{33} mode, several thin slices of PZT are stacked together and separated by electrodes; the direction of expansion is parallel to the electric field.

ii) In the in-plane or d_{31} mode, a thin piezoelectric film is bonded on (or embedded in) a plate structure and creates a bending moment. The direction of expansion is perpendicular to the electric field.

iii) In the shear or d_{15} mode, the electric field is applied perpendicular to the polarization direction.

Considering these three effects, d matrix can be written as

$$
d = \begin{bmatrix}
0 & 0 & 0 & 0 & d_{15} & 0 \\
0 & 0 & 0 & d_{24} & 0 & 0 \\
d_{31} & d_{32} & d_{33} & 0 & 0 & 0
\end{bmatrix} = \begin{bmatrix}
0 & 0 & 0 & 0 & d_{15} & 0 \\
0 & 0 & 0 & d_{15} & 0 & 0 \\
d_{31} & d_{31} & d_{33} & 0 & 0 & 0
\end{bmatrix}
$$

then e matrix becomes

$$e = cd^T = \begin{bmatrix} c_{11} & c_{12} & c_{13} & 0 & 0 & 0 \\ c_{12} & c_{11} & c_{13} & 0 & 0 & 0 \\ c_{13} & c_{13} & c_{33}, & 0 & 0 & 0 \\ 0 & 0 & 0 & c_{44} & 0 & 0 \\ 0 & 0 & 0 & 0 & c_{44} & 0 \\ 0 & 0 & 0 & 0 & 0 & 2(c_{11}-c_{12}) \end{bmatrix} \begin{bmatrix} 0 & 0 & d_{31} \\ 0 & 0 & d_{31} \\ 0 & 0 & d_{33} \\ 0 & d_{15} & 0 \\ d_{15} & 0 & 0 \\ 0 & 0 & 0 \end{bmatrix}$$

$$= \begin{bmatrix} 0 & 0 & c_{11}d_{31}+c_{12}d_{31}+c_{13}d_{33} \\ 0 & 0 & c_{12}d_{31}+c_{11}d_{31}+c_{13}d_{33} \\ 0 & 0 & c_{13}d_{31}+c_{13}d_{31}+c_{33}d_{33} \\ 0 & c_{44}d_{15} & 0 \\ c_{44}d_{15} & 0 & 0 \\ 0 & 0 & 0 \end{bmatrix}$$

$$= \begin{bmatrix} 0 & 0 & e_{13} \\ 0 & 0 & e_{13} \\ 0 & 0 & e_{33} \\ 0 & e_{42} & 0 \\ e_{42} & 0 & 0 \\ 0 & 0 & 0 \end{bmatrix}$$

- ε is the matrix of dielectric constants, given as

$$\varepsilon = \begin{bmatrix} \varepsilon_{11} & 0 & 0 \\ 0 & \varepsilon_{22} & 0 \\ 0 & 0 & \varepsilon_{33} \end{bmatrix}$$

here, ε_{11} and ε_{22} are permittivities for dielectric displacement and electric field in direction 1 and 2 (perpendicular to the direction in which ceramic element is polarized), ε_{33} is the permittivity for dielectric displacement and electric field in direction 3 (parallel to the direction in which ceramic element is polarized).

These equations are suitable for finite element packages because the displacements (and hence the strains) are the independent variables, whereas the boundary conditions are given as force loadings, that is as stresses in these packages.

As a result, the following properties entered for the piezoelectric patches to ABAQUS: Density, Young's modulus, Poisson's ratio, structural damping, piezoelectric coefficients (d_{31}, d_{33}, d_{15}), dielectric constants (ε_{11}, ε_{22}, ε_{33}) and elasticity matrix coefficients (c_{11}, c_{33}, c_{44}, c_{12}, c_{13}). The corresponding values are provided by the manufacturer.

Appendix B

BLOCK DIAGRAM USED IN THE USER STUDIES
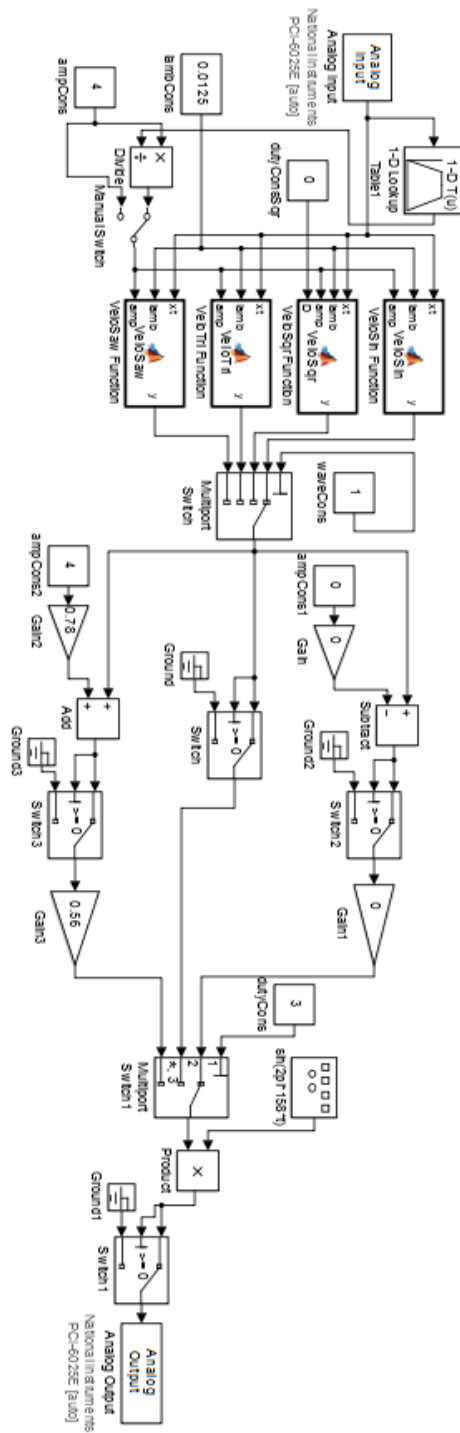
Appendix C

INSTRUCTIONS USED IN THE EXPERIMENT

- Thank you for agreeing to participate in this study.

- Please read through these instructions and ask any question you may have **<u>before</u>** the experiment begins.

- Please turn off any electronic devices before the experiment begins.

- In this experiment you will be presented some haptic (touch based) signals. You will explore these signals by moving your finger on a surface.

- You will be given white noise via headphones during the experiment. The noise might be little disturbing. Please **<u>do not remove</u>** your headphones during the experiment.

- You need to use your both hands during the experiment.

- While you are exploring the surface with your right hand, you will enter your decision about the roughness and bumpiness of the surface using your left hand.

- You will use your right hand's index finger to explore the surface.

- You will use your left hand to enter your decision to the screen using a pen.

- Roughness:

  Smooth surface: An even surface <u>free from irregularities</u>
  Rough surface: An uneven surface <u>with irregularities, changes in the amplitude</u>
  For the roughness bar
      1 stands for the smoothest surface
      7 stands for the roughest surface

- Bumpiness:

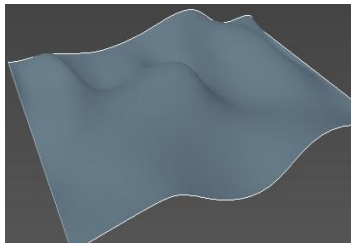 Flat surface: A surface with <u>no bumps</u>

  Bumpy surface: A surface with <u>countable bumps</u>

  For the bumpiness bar

        1 stands for the flattest surface

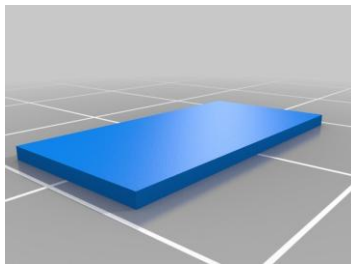   7 stands for the bumpiest surface

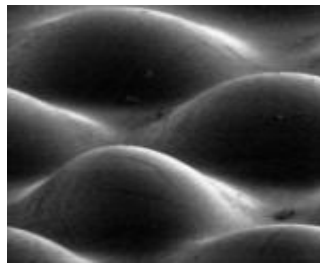- Some examples

Smooth   Rough

Flat   Bumpy

- First you will be given a trial session with 48 signals and then the real experiment will start.

- You can explore each signal only for 15 seconds and **<u>you can replay each signal only once</u>**. So it is important to make your decision at this limited time interval.

- When you click on the NEXT button, next signal will be displayed to you through the surface.

- You can change your decisions about the roughness and bumpiness scales until you press the NEXT button.

- You can ask any questions you have during the trial session.

- Please **do not ask any questions** during the experiment.

- Please not that there is no "right answer" for this experiment. It is important to mark the option that best fits to you

- Thank you for your participation!